

# CHAPTER 19

## SIMPLIFIED SOLUTIONS FOR STRESSES AND DEFORMATIONS

In the preceding chapters the solid surfaces in a lubricated conjunction have been considered to be rigid. This then is the demarcation point where elastic deformation of the solid surfaces will begin to be considered and remain of concern until the end of the book.

The classical Hertzian solution for deformation requires calculating the ellipticity parameter  $k$  and the complete elliptic integrals of the first and second kinds  $\mathcal{F}$  and  $\mathcal{E}$ , respectively. Simplifying expressions for  $k$ ,  $\mathcal{F}$ , and  $\mathcal{E}$  as a function of the radius ratio  $\alpha_r$  were presented by Brewe and Hamrock (1977) in a curve-fit analysis. With these expressions researchers could determine the deformation at the contact center, with a slight sacrifice in accuracy, without using involved mathematical methods or design charts. The simplified expressions were useful for radius ratios ranging from circular point contact to near line contact normal to the rolling direction (that is,  $1.0 \leq \alpha_r \leq 100$ ).

However, in a number of applications the semimajor axis of the elliptical contact is parallel to the rolling direction, resulting in  $\alpha_r < 1$ . Some of these applications are (1) Novikov gear contacts, (2) locomotive wheel-rail contacts, and (3) roller-flange contacts in an axial loaded roller bearing. The elliptical contact deformation and stresses presented by Hamrock and Brewe (1983) are applicable for any contact ranging from something similar to a disk rolling

on a plane ( $\alpha_r = 0.03$ ) to a ball-on-plane contact ( $\alpha_r = 1$ ) to a contact approaching a nominal line contact ( $\alpha_r \rightarrow 100$ ) such as a barrel-shaped roller bearing against a plane. This chapter focuses on the results obtained by Hamrock and Brewe in their 1983 paper.

### 19.1 CURVATURE SUM AND DIFFERENCE

The undeformed geometry of nonconformal contacting solids can be represented in general terms by two ellipsoids, as shown in Fig. 19.1. The two solids with different radii of curvature in a pair of principal planes ( $x$  and  $y$ ) passing through the contact between the solids make contact at a single point under the condition of zero applied load. Such a condition is called "point contact" and is shown in Fig. 19.1, where the radii of curvature are denoted by  $r$ 's. It is assumed throughout this book that convex surfaces, as shown in Fig. 19.1, exhibit positive curvature and concave surfaces, negative curvature. Therefore, if the center of curvature lies within the solid, the radius of curvature is positive; if the center of curvature lies outside the solid, the radius of curvature is negative. Figure 19.2 shows the sign designations for the radii of curvature for various machine elements such as rolling elements and bearing races. The importance of the sign of the radius of curvature presents itself later in the chapter.

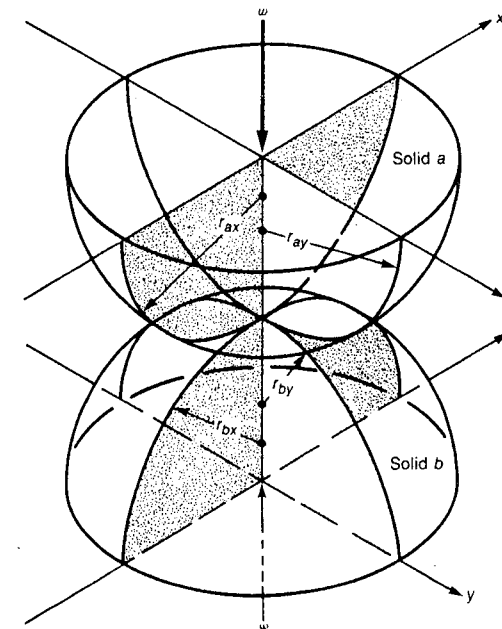
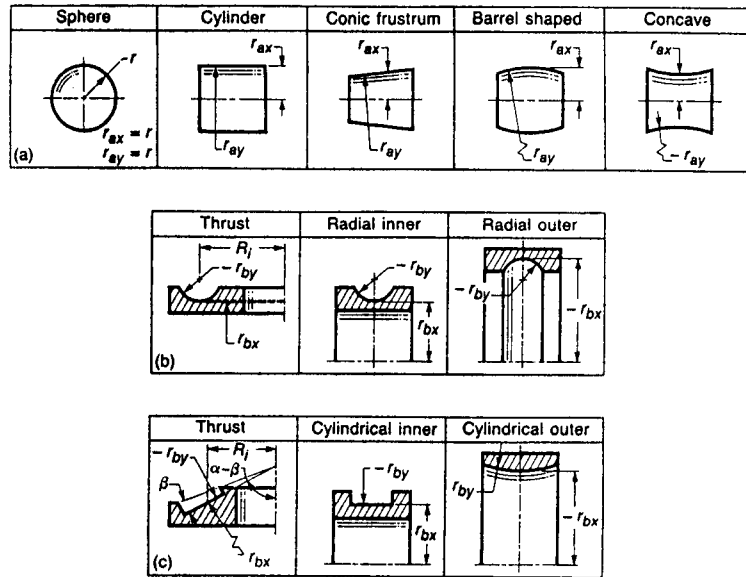


FIGURE 19.1  
Geometry of contacting elastic solids.  
[From Hamrock and Dowson (1981).]



**FIGURE 19.2** Sign designations for radii of curvature of various machine elements. (a) Rolling elements; (b) ball bearing races; (c) rolling bearing races.

Note that if coordinates  $x$  and  $y$  are chosen such that

$$\frac{1}{r_{ax}} + \frac{1}{r_{bx}} \geq \frac{1}{r_{ay}} + \frac{1}{r_{by}} \tag{19.1}$$

coordinate  $x$  then determines the direction of the semiminor axis of the contact area when a load is applied and  $y$ , the direction of the semimajor axis. The direction of the entraining motion is always considered to be along the  $x$  axis. For those situations in which the principal curvature planes of the two contacting bodies are not coincident, refer to Timoshenko and Goodier (1970).

The curvature sum and difference, which are quantities of some importance in analyzing contact stresses and deformation, are

$$\frac{1}{R} = \frac{1}{R_x} + \frac{1}{R_y} \tag{19.2}$$

$$R_d = R \left( \frac{1}{R_x} - \frac{1}{R_y} \right) \tag{19.3}$$

where

$$\frac{1}{R_x} = \frac{1}{r_{ax}} + \frac{1}{r_{bx}} \tag{19.4}$$

$$\frac{1}{R_y} = \frac{1}{r_{ay}} + \frac{1}{r_{by}} \tag{19.5}$$

Equations (19.4) and (19.5) effectively redefine the problem of two ellipsoidal solids approaching one another in terms of an equivalent solid of radii  $R_x$  and  $R_y$  approaching a plane. Note that the curvature difference expressed in Eq. (19.3) is dimensionless.

The radius ratio  $\alpha_r$  defined in Eq. (18.57) is the same for this chapter.

$$\therefore \alpha_r = \frac{R_y}{R_x} \tag{18.57}$$

Thus, if Eq. (19.1) is satisfied,  $\alpha_r > 1$ ; and if it is not satisfied,  $\alpha_r < 1$ .

## 19.2 SURFACE STRESSES AND DEFORMATIONS

When an elastic solid is subjected to a load, stresses are produced that increase as the load is increased. These stresses are associated with deformations, which are defined by strains. Unique relationships exist between stresses and their corresponding strains. For elastic solids the stresses are linearly related to the strains, with the constant of proportionality being an elastic constant that adopts different values for different materials as covered in Sec. 5.6.2. The modulus of elasticity  $E$  and Poisson's ratio  $\nu$  are two important parameters described in Chap. 5 that are used in this chapter to describe contacting solids.

As the stresses increase within the material, elastic behavior is replaced by plastic flow in which the material is permanently deformed. The stress state at which the transition from elastic to plastic behavior occurs, known as the "yield stress," has a definite value for a given material at a given temperature. In this book only elastic behavior is considered.

When two elastic solids are brought together under a load, a contact area develops whose shape and size depend on the applied load, the elastic properties of the materials, and the curvatures of the surfaces. When the two solids shown in Fig. 19.1 have a normal load applied to them, the contact area is elliptical. It has been common to refer to elliptical contacts as point contacts, but since under load these contacts become elliptical, they are referred to herein as such. For the special case where  $r_{ax} = r_{ay}$  and  $r_{bx} = r_{by}$  the resulting contact is a circle rather than an ellipse. Where  $r_{ay}$  and  $r_{by}$  are both infinite, the initial line contact develops into a rectangle when load is applied.

Hertz (1881) considered the stresses and deformations in two perfectly smooth, ellipsoidal, contacting solids much like those shown in Fig. 19.1. His application of the classical elasticity theory to this problem forms the basis of

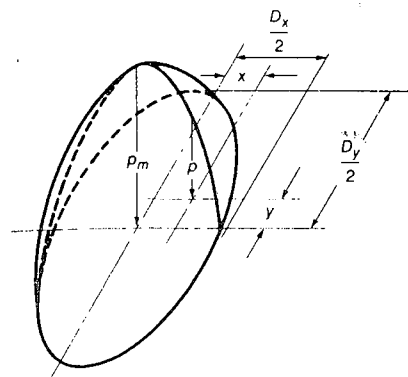


FIGURE 19.3  
Pressure distribution in ellipsoidal contact.

stress calculations for machine elements such as ball and roller bearings, gears, and cams and followers. Hertz made the following assumptions:

1. The materials are homogeneous and the yield stress is not exceeded.
2. No tangential forces are induced between the solids.
3. Contact is limited to a small portion of the surface such that the dimensions of the contact region are small in comparison with the radii of the ellipsoids.
4. The solids are at rest and in equilibrium.

Making use of these assumptions, Hertz (1881) was able to obtain the following expression for the pressure within the ellipsoidal contact (shown in Fig. 19.3):

$$p = p_m \left[ 1 - \left( \frac{2x}{D_x} \right)^2 - \left( \frac{2y}{D_y} \right)^2 \right]^{1/2} \quad (19.6)$$

where  $D_x$  = diameter of contact ellipse in  $x$  direction, m  
 $D_y$  = diameter of contact ellipse in  $y$  direction, m

If the pressure is integrated over the contact area, it is found that

$$p_m = \frac{6w_z}{\pi D_x D_y} \quad (19.7)$$

where  $w_z$  is the normal applied load. Equation (19.6) determines the distribution of pressure or compressive stress on the common interface; it is clearly a maximum at the contact center and decreases to zero at the periphery.

The ellipticity parameter  $k$  is defined as the elliptical contact diameter in the  $y$  direction (transverse direction) divided by the elliptical contact diameter

in the  $x$  direction (direction of entraining motion), or

$$k = \frac{D_y}{D_x} \quad (19.8)$$

If Eq. (19.1) is satisfied and  $\alpha_r \geq 1$ , the contact ellipse will be oriented with its major diameter transverse to the direction of motion, and consequently  $k \geq 1$ . Otherwise, the major diameter would lie along the direction of motion with both  $\alpha_r < 1$  and  $k < 1$ . To avoid confusion, the commonly used solutions to the surface deformation and stresses are presented only for  $\alpha_r > 1$ . The simplified solutions are presented, and then their application for  $\alpha_r < 1$  is discussed.

Harris (1966) has shown that the ellipticity parameter can be written as a transcendental equation relating the curvature difference [Eq. (19.3)] and the elliptic integrals of the first  $\mathcal{F}$  and second  $\mathcal{E}$  kinds as

$$k = \left[ \frac{2\mathcal{F} - \mathcal{E}(1 + R_d)}{\mathcal{E}(1 - R_d)} \right]^{1/2} \quad (19.9)$$

where

$$\mathcal{F} = \int_0^{\pi/2} \left[ 1 - \left( 1 - \frac{1}{k^2} \right) \sin^2 \phi \right]^{-1/2} d\phi \quad (19.10)$$

$$\mathcal{E} = \int_0^{\pi/2} \left[ 1 - \left( 1 - \frac{1}{k^2} \right) \sin^2 \phi \right]^{1/2} d\phi \quad (19.11)$$

A one-point iteration method that was adopted by Hamrock and Anderson (1973) can be used to obtain the ellipticity parameter, where

$$k_{n+1} \cong k_n \quad (19.12)$$

The iteration process is normally continued until  $k_{n+1}$  differs from  $k_n$  by less than  $1.0 \times 10^{-7}$ . Note that the ellipticity parameter is a function only of the solids' radii of curvature:

$$k = f(r_{ax}, r_{bx}, r_{ay}, r_{by}) \quad (19.13)$$

That is, as the load increases, the semiaxes in the  $x$  and  $y$  directions of the contact ellipse increase proportionately to each other so that the ellipticity parameter remains constant.

Figure 19.4 shows the ellipticity parameter and the elliptic integrals of the first and second kinds for a radius ratio ( $\alpha_r = R_y/R_x$ ) range usually encountered in nonconformal conjunctions. Note from Fig. 19.4 that  $\mathcal{E} = \mathcal{F}$  when  $\alpha_r = 1$ . Also both  $\mathcal{E}$  and  $\mathcal{F}$  are discontinuous at  $\alpha_r = 1$ .

When the ellipticity parameter  $k$ , the normal applied load  $w_z$ , Poisson's ratio  $\nu$ , and the modulus of elasticity  $E$  of the contacting solids are known, the major and minor axes of the contact ellipse and the maximum deformation at

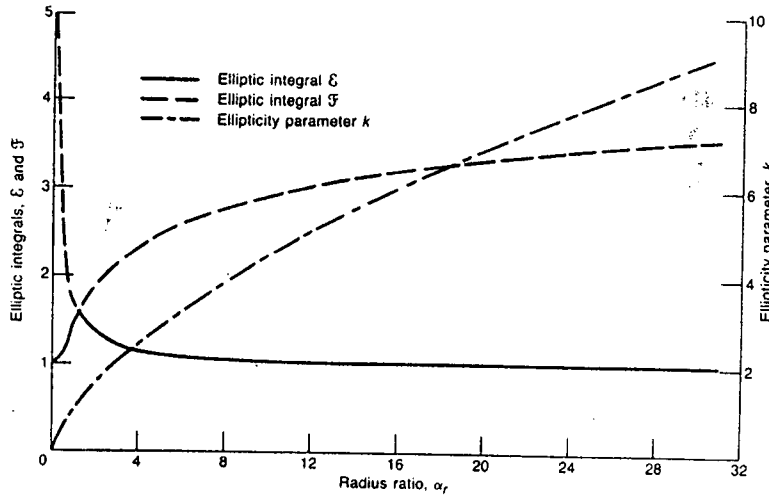


FIGURE 19.4 Variation of ellipticity parameter and elliptic integrals of first and second kinds as function of radius ratio. [From Hamrock and Brewe (1983).]

the contact center can be written from the analysis of Hertz (1881) as

$$D_y = 2 \left( \frac{6k^2 \mathcal{E} w_z R}{\pi E'} \right)^{1/3} \quad (19.14)$$

$$D_x = 2 \left( \frac{6 \mathcal{E} w_z R}{\pi k E'} \right)^{1/3} \quad (19.15)$$

$$\delta_m = \mathcal{F} \left[ \frac{9}{2 \mathcal{E} R} \left( \frac{w_z}{\pi k E'} \right)^2 \right]^{1/3} \quad (19.16)$$

where

$$E' = \frac{2}{(1 - \nu_a^2)/E_a + (1 - \nu_b^2)/E_b} \quad (19.17)$$

In these equations,  $D_x$  and  $D_y$  are proportional to  $w_z^{1/3}$  and  $\delta_m$  is proportional to  $w_z^{2/3}$ .

### 19.3 SUBSURFACE STRESSES

Fatigue cracks usually start at a certain depth below the surface in planes parallel to the rolling direction. Because of this, special attention must be given to the shear stress amplitude in this plane. Furthermore, a maximum shear stress is reached at a certain depth below the surface. The analysis used by Lundberg and Palmgren (1947) is used here to define this stress.

The stresses are referred to in a rectangular coordinate system with its origin at the contact center, its  $z$  axis coinciding with the interior normal of the body considered, its  $x$  axis in the rolling direction, and its  $y$  axis perpendicular to the rolling direction. In the analysis that follows, it is assumed that  $y = 0$ .

From Lundberg and Palmgren (1947) the following equations can be written:

$$\tau_{zx} = \frac{6 w_z \cos^2 \phi_a \sin \phi_a \sin \gamma_a}{\pi (D_y^2 \tan^2 \gamma_a + D_x^2 \cos^2 \phi_a)} \quad (19.18)$$

$$x = \frac{1}{2} (D_x^2 + D_y^2 \tan^2 \gamma_a)^{1/2} \sin \phi_a \quad (19.19)$$

$$z = \frac{D_y}{2} \tan \gamma_a \cos \phi_a \quad (19.20)$$

where  $\phi_a$  and  $\gamma_a$  are auxiliary angles used in place of the coordinate set  $(x, z)$ . They are defined so as to satisfy the relationship of a conformal ellipsoid to the pressure ellipse (for further details see Hertz, 1881, and Lundberg and Palmgren, 1947).

The maximum shear stress is defined as

$$\tau_0 = (\tau_{zx})_{\max}$$

The amplitude of  $\tau_0$  is obtained from

$$\frac{\partial \tau_{zx}}{\partial \phi_a} = 0 \quad \frac{\partial \tau_{zx}}{\partial \gamma_a} = 0$$

For the point of maximum shear stress

$$\tan^2 \phi_a = t^* \quad (19.21)$$

$$\tan^2 \gamma_a = t^* - 1 \quad (19.22)$$

$$\frac{D_x}{D_y} = \left\{ [(t^*)^2 - 1] (2t^* - 1) \right\}^{1/2} \quad (19.23)$$

where  $t^*$  is the auxiliary parameter. The position of the maximum point is determined by

$$z_0 = \xi^* \frac{D_x}{2} \quad (19.24)$$

$$x_0 = \pm \xi^* \frac{D_x}{2} \quad (19.25)$$

where

$$\xi^* = \frac{1}{(t^* + 1)(2t^* - 1)^{1/2}} \quad (19.26)$$

$$\xi^* = \frac{t^*}{t^* + 1} \left( \frac{2t^* + 1}{2t^* - 1} \right)^{1/2} \quad (19.27)$$

Furthermore, the magnitude of the maximum shear stress expressed in terms of  $t^*$  is given by

$$\tau_0 = p_m \frac{(2t^* - 1)^{1/2}}{2t^*(t^* + 1)} \quad (19.28)$$

It should be emphasized that  $\tau_0$  represents the maximum half-amplitude of the subsurface orthogonal shear stress and is not to be confused with the maximum subsurface shear stress that occurs below the center of the contact on the plane oriented  $45^\circ$  to the surface. The Lundberg-Palmgren prediction of fatigue life is based on the calculation of  $\tau_0$  and was limited to cross sections lying in the plane of symmetry of the roller path ( $y = 0$ ).

#### 19.4 SIMPLIFIED SOLUTIONS

The classical Hertzian solution presented in the previous sections requires the calculation of the ellipticity parameter  $k$  and the complete elliptic integrals of the first and second kinds  $\mathcal{F}$  and  $\mathcal{E}$ . This entails finding a solution to a transcendental equation relating  $k$ ,  $\mathcal{F}$ , and  $\mathcal{E}$  to the geometry of the contacting solids, as expressed in Eq. (19.9). This is usually accomplished by some iterative numerical procedure, as described by Hamrock and Anderson (1973), or with the aid of charts, as shown by Jones (1946).

Table 19.1 shows various radius ratios  $\alpha_r$  and corresponding values of  $k$ ,  $\mathcal{F}$ , and  $\mathcal{E}$  obtained from the numerical procedure given in Hamrock and Anderson (1973). Hamrock and Brewe (1983) used a linear regression by the method of least squares to power fit the set of pairs of data  $[(k_i, \alpha_{r,i}), i = 1, 2, \dots, 26]$  shown in Table 19.1. They obtained the following equation:

$$\bar{k} = \alpha_r^{2/\pi} \quad (19.29)$$

The asymptotic behavior of  $\mathcal{E}$  and  $\mathcal{F}$  ( $\alpha_r \rightarrow 1$  implies  $\mathcal{E} \rightarrow \mathcal{F} \rightarrow \pi/2$ , and  $\alpha_r \rightarrow \infty$  implies  $\mathcal{F} \rightarrow \infty$  and  $\mathcal{E} \rightarrow 1$ ) was suggestive of the type of functional dependence that  $\bar{\mathcal{E}}$  and  $\bar{\mathcal{F}}$  might follow. As a result, both inverse and logarithmic curve fits were tried for  $\bar{\mathcal{E}}$  and  $\bar{\mathcal{F}}$ , respectively. Hamrock and Brewe (1983) obtained the following:

$$\bar{\mathcal{E}} = 1 + \frac{q_a}{\alpha_r} \quad \text{for } \alpha_r \geq 1 \quad (19.30)$$

where 
$$q_a = \frac{\pi}{2} - 1 \quad (19.31)$$

and 
$$\bar{\mathcal{F}} = \frac{\pi}{2} + q_a \ln \alpha_r \quad \text{for } \alpha_r \geq 1 \quad (19.32)$$

Values of  $\bar{k}$ ,  $\bar{\mathcal{E}}$ , and  $\bar{\mathcal{F}}$  are also presented in Table 19.1 and compared with the numerically determined values of  $k$ ,  $\mathcal{E}$ , and  $\mathcal{F}$ . Table 19.1 also gives the

TABLE 19.1  
Comparison of numerically determined values with curve-fit values for geometrically dependent variables

[From Hamrock and Brewe (1983);  $R_x = 1.0$  cm]

Radius ratio, $\alpha_r$	Ellipticity			Complete elliptic integral of first kind			Complete elliptic integral of second kind		
	$k$	$\bar{k}$	Error, $e_r$ , percent	$\mathcal{F}$	$\bar{\mathcal{F}}$	Error, $e_r$ , percent	$\mathcal{E}$	$\bar{\mathcal{E}}$	Error, $e_r$ , percent
1.00	1.00	1.00	0	1.57	1.57	0	1.57	1.57	0
1.25	1.16	1.15	.66	1.68	1.69	-.50	1.46	1.45	.52
1.50	1.31	1.29	1.19	1.78	1.80	-.70	1.39	1.38	.76
1.75	1.45	1.42	1.61	1.87	1.89	-.75	1.33	1.32	.87
2.00	1.58	1.55	1.96	1.95	1.96	-.73	1.29	1.28	.91
3.00	2.07	2.01	2.87	2.18	2.19	-.44	1.20	1.19	.83
4.00	2.50	2.41	3.35	2.35	2.36	-.11	1.15	1.14	.69
5.00	2.89	2.78	3.61	2.49	2.48	.17	1.12	1.11	.57
6.00	3.25	3.12	3.74	2.60	2.59	.40	1.10	1.09	.48
7.00	3.58	3.45	3.80	2.69	2.68	.59	1.08	1.08	.40
8.00	3.90	3.75	3.81	2.77	2.75	.75	1.07	1.07	.35
9.00	4.20	4.05	3.78	2.85	2.82	.88	1.06	1.06	.30
10.00	4.49	4.33	3.74	2.91	2.88	1.00	1.05	1.05	.26
15.00	5.79	5.60	3.32	3.16	3.11	1.38	1.03	1.03	.15
20.00	6.92	6.73	2.81	3.33	3.28	1.60	1.02	1.02	.10
25.00	7.94	7.76	2.29	3.46	3.40	1.74	1.02	1.02	.07
30.00	8.87	8.71	1.79	3.57	3.51	1.84	1.01	1.01	.05
35.00	9.74	9.61	1.32	3.67	3.60	1.90			.04
40.00	10.56	10.46	.87	3.74	3.67	1.95			.03
45.00	11.33	11.28	.44	3.81	3.74	1.99			.02
50.00	12.07	12.06	.03	3.88	3.80	2.02			.02
60.00	13.45	13.52	-.72	3.98	3.90	2.06	1.00	1.00	.01
70.00	14.74	14.94	-1.40	4.08	3.99	2.08			.01
80.00	15.95	16.27	-2.03	4.15	4.07	2.09			.01
90.00	17.09	17.54	-2.61	4.22	4.13	2.10			0
100.00	18.18	18.76	-3.15	4.28	4.19	2.10			0

percentage of error determined as

$$e_r = \frac{(\bar{i} - i)100}{i} \quad (19.33)$$

where

$$i = \{k, \mathcal{E}, \text{ or } \mathcal{F}\} \quad (19.34)$$

$$\bar{i} = \{\bar{k}, \bar{\mathcal{E}}, \text{ or } \bar{\mathcal{F}}\} \quad (19.35)$$

The agreement between the exact solution and the approximate formulas is quite good. The best agreement is with  $\mathcal{E}$ , which is between 0 and 1 percent; the worst agreement is with  $k$ , which is  $\pm 4$  percent.

**TABLE 19.2**  
Effect of radius ratio on auxiliary parameter used in subsurface stress calculations

[From Hamrock and Brewe (1983)]

Radius ratio, $\alpha_r$	Auxiliary parameter			Radius ratio, $\alpha_r$	Auxiliary parameter		
	$t^*$	$\bar{t}^*$	Error, $e_r$ , percent		$t^*$	$\bar{t}^*$	Error, $e_r$ , percent
0.01	5.71	7.00	-22.47	2.00	1.14	1.18	-3.71
.02	4.42	4.86	-9.87	3.00	1.09	1.13	-3.78
.03	3.81	3.98	-4.49	4.00	1.06	1.10	-3.45
.04	3.43	3.48	-1.51	5.00	1.05	1.08	-3.03
.05	3.16	3.15	.35	6.00	1.04	1.07	-2.62
.06	2.96	2.91	1.58	7.00	1.03	1.05	-2.24
.07	2.80	2.73	2.42	8.00	1.03	1.05	-1.91
.08	2.67	2.59	3.01	9.00	1.02	1.04	-1.61
.09	2.56	2.47	3.43	10.00	1.02	1.03	-1.35
.10	2.47	2.38	3.72	15.00	1.01	1.01	-.50
.20	1.96	1.88	3.90	20.00	1.00	1.01	-.09
.30	1.73	1.68	2.86	25.00		1.00	.12
.40	1.59	1.56	1.79	30.00			.21
.50	1.50	1.48	.85	35.00			.26
.60	1.43	1.43	.05	40.00			.27
.70	1.38	1.39	-.62	45.00			.27
.80	1.34	1.35	-1.19	50.00			.26
.90	1.30	1.33	-1.66	60.00			.24
1.00	1.28	1.30	-2.05	70.00			.21
1.25	1.22	1.26	-2.78	80.00			.19
1.50	1.19	1.23	-3.25	90.00			.17
1.75	1.16	1.20	-3.54	100.00			.15

Table 19.2 shows various radius ratios  $\alpha_r$ , and corresponding values of the auxiliary parameter  $t^*$  used in calculating the position and value of the maximum subsurface orthogonal shear stress. The exact solution for  $t^*$  was obtained from the numerical procedures given in Hamrock and Anderson (1973). For the set of data  $[(t_i^*, \alpha_{r,i}), i = 1, 2, \dots, 44]$  shown in Table 19.2 the following simplified formula was obtained from Hamrock and Brewe (1983):

$$\bar{t}^* = 1 + 0.16 \operatorname{csch} \frac{\bar{k}}{2} \quad (19.36)$$

The percentage of error  $e_r$  is given for the auxiliary parameter in Table 19.2. The agreement between the exact and the approximate values of  $t^*$  is quite good except at extremely small radius ratios ( $\alpha_r \leq 0.03$ ). Once the value of  $t^*$  is determined, the position and value of the maximum subsurface orthogonal shear stress can readily be calculated from Eqs. (19.24) to (19.28).

**TABLE 19.3**  
Simplified equations

[From Hamrock and Brewe (1983)]

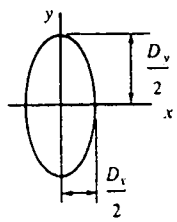
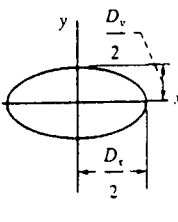
Diagram	Equations
	$1 \leq \alpha_r \leq 100$ $\bar{k} = \alpha_r^{2/\pi}$ $\bar{\mathcal{F}} = \frac{\pi}{2} + q_a \ln \alpha_r$ where $q_a = \frac{\pi}{2} - 1$ $\bar{\mathcal{E}} = 1 + \frac{q_a}{\alpha_r}$ $\bar{t}^* = 1 + 0.16 \operatorname{csch} \left( \frac{\bar{k}}{2} \right)$
	$0.01 \leq \alpha_r \leq 1.0$ $\bar{k} = \alpha_r^{2/\pi}$ $\bar{\mathcal{F}} = \frac{\pi}{2} - q_a \ln \alpha_r$ where $q_a = \frac{\pi}{2} - 1$ $\bar{\mathcal{E}} = 1 + q_a \alpha_r$ $\bar{t}^* = 1 + 0.16 \operatorname{csch} \left( \frac{\bar{k}}{2} \right)$

Table 19.3, from Hamrock and Brewe (1983), gives the simplified equations for  $0.01 \leq \alpha_r \leq 100$ , which is the complete range normally experienced in practice. It is important to make the proper evaluation of  $\alpha_r$ , since it has great significance in the outcome of the simplified equations. Table 19.3 shows that  $\bar{k}$  and  $\bar{t}^*$  are unaffected by the orientation of the ellipse but that the elliptical integrals of the first and second kinds ( $\mathcal{F}$  and  $\mathcal{E}$ ) are quite affected. It is important to realize that the reciprocal to  $\alpha_r$  produces the same values of  $\bar{k}$  and  $\bar{\mathcal{E}}$  as are produced by changing the orientation of the ellipse.

Figure 19.5 shows three diverse situations in which the simplified equations can be usefully applied. The locomotive wheel on a rail [Fig. 19.5(a)] illustrates an example in which the ellipticity parameter  $k$  and the radius ratio  $\alpha_r$  are less than 1. The ball rolling against a plane [Fig. 19.5(b)] provides a pure circular contact (i.e.,  $\alpha_r = k = 1.00$ ). Figure 19.5(c) shows how the contact ellipse is formed in the ball-outer-race contact of a ball bearing. Here the semimajor axis is normal to the rolling direction, and consequently  $\alpha_r$  and  $k$  are greater than 1. The detailed geometry and the values that can be calculated from the simplified formulas are given in Table 19.4 for each of these three configurations. In using these formulas it is important to pay attention to the

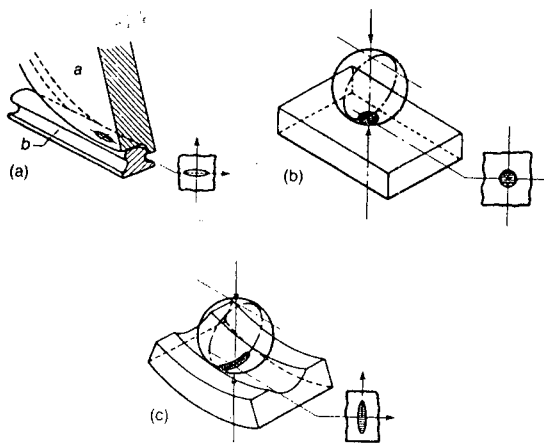


FIGURE 19.5 Three degrees of conformity. (a) Wheel on rail; (b) ball on plane; (c) ball-outer-race contact. [From Hamrock and Brewe (1983).]

sign of the curvatures. Note that the outer race in Fig. 19.5 is a concave surface and therefore requires a negative sign. Table 19.4 shows both the maximum pressure  $p_m$  and the maximum shear stress to be highest for the ball-on-plane configuration.

19.5 RECTANGULAR CONJUNCTIONS

For rectangular conjunctions the contact ellipse discussed throughout this chapter is of infinite width in the transverse direction ( $D_y \rightarrow \infty$ ). This type of contact is exemplified by a cylinder loaded against a plane, a groove, or another parallel cylinder or by a roller loaded against an inner or outer race. In these situations the contact semiwidth is given by

$$b^* = R_x \left( \frac{8W'}{\pi} \right)^{1/2} \tag{19.37}$$

where the dimensionless load is

$$W' = \frac{w'}{E'R_x} \tag{19.38}$$

and  $w'$  is the load per unit width along the contact. The maximum deformation for a rectangular conjunction can be written as

$$\delta_m = \frac{2W'R_x}{\pi} \left[ \ln \left( \frac{2\pi}{W'} \right) - 1 \right] \tag{19.39}$$

The maximum Hertzian pressure in a rectangular conjunction can be written as

$$p_H = E' \left( \frac{W'}{2\pi} \right)^{1/2}$$

TABLE 19.4 Practical applications for differing conformities

[From Hamrock and Brewe (1983); effective elastic modulus  $E', 2.197 \times 10^{11}$  Pa]

Contact parameters	Wheel on rail	Ball on plane	Ball-outer-race contact
$w', N$	$1.00 \times 10^5$	222.4111	222.4111
$r_{ax}, m$	0.5019	0.006350	0.006350
$r_{ay}, m$	$\infty$	0.006350	0.006350
$r_{bx}, m$	$\infty$	$\infty$	-0.038900
$r_{by}, m$	0.300000	$\infty$	-0.006600
$\alpha_r$	0.5977	1.0000	22.0905
$k$	0.7099	1.0000	7.3649
$\bar{k}$	0.7206	1.0000	7.1738
$\mathcal{E}$	1.3526	1.5708	1.0267
$\bar{\mathcal{E}}$	1.3412	1.5708	1.0258
$\mathcal{F}$	1.8508	1.5708	3.3941
$\bar{\mathcal{F}}$	1.8645	1.5708	3.3375
$D_x, m$	0.010783	0.000426	0.001842
$\bar{D}_x, m$	0.010807	0.000426	0.001810
$D_y, m$	0.015190	0.000426	0.000250
$\bar{D}_y, m$	0.014996	0.000426	0.000252
$\delta_m, \mu m$	106	7.13	3.56
$\bar{\delta}_m, \mu m$	108	7.13	3.57
$p_m, GPa$	1.166	2.34	0.922
$\bar{p}_m, GPa$	1.178	2.34	0.930
$i^*$	1.4354	1.2808	1.0090
$\bar{i}^*$	1.4346	1.3070	1.0089
$x_0, m$	$\pm 0.008862$	$\pm 0.000195$	$\pm 0.000096$
$\bar{x}_0, m$	$\pm 0.008745$	$\pm 0.000197$	$\pm 0.000097$
$z_0, m$	$\pm 0.005410$	$\pm 0.000149$	$\pm 0.000123$
$\bar{z}_0, m$	$\pm 0.005350$	$\pm 0.000145$	$\pm 0.000124$
$\tau_0, GPa$	0.162	0.501	0.229
$\bar{\tau}_0, GPa$	0.164	0.494	0.232

19.6 CLOSURE

This chapter has presented an alternative approach to the classical Hertzian solution for the local stress and deformation of two elastic bodies in contact. Simplified formulas that use curve-fit analysis are given in terms of the radius ratio  $\alpha_r$  for the ellipticity parameter  $k$  and the complete integrals  $\mathcal{F}$  and  $\mathcal{E}$  of the first and second kinds, respectively. Thus, their interdependence can be uncoupled and solution of the resulting transcendental equation avoided. Simplified equations were developed that permit a more direct and easier approach to the calculation of the elliptical contact deformation and the maximum

Hertzian pressure. In addition, a curve-fit analysis was used to derive a simplified formula for an auxiliary parameter  $t^*$  as a function of  $\alpha_r$ . This eliminated having to solve a cubic equation for  $t^*$  as a function of  $k$ . A shortcut calculation could be made for the location and magnitude of the maximum subsurface shear stress. Therefore, the elliptical contact deformation and stresses presented are applicable for any contact ranging from a disk rolling on a plane ( $\alpha_r = 0.03$ ) to a ball-on-plane contact ( $\alpha_r = 1$ ) to a contact approaching a normal line contact ( $\alpha_r \rightarrow 100$ ) such as a barrel-shaped roller against a plane.

## 19.7 PROBLEMS

19.7.1 A solid cylinder of radius 2 cm rolls around an inner ring with an internal radius of 10 cm and a large width in the axial ( $y$ ) direction. What is the radius of the geometrically equivalent cylinder near a plane?

The cylinder is made of silicon nitride and the ring is made of stainless steel. If a normal applied load per unit width is 1,000 N/m determine the contact semiwidth  $b^*$ , maximum deformation  $\delta_m$ , and maximum Hertzian pressure  $p_H$ . Also indicate what these values are if the silicon nitride cylinder is replaced with a stainless steel cylinder. What conclusions can you make about these results?

19.7.2 A solid sphere of radius 2 cm rolls around the inner ring with an internal radius of 10 cm and a large width in the axial ( $y$ ) is quite large. What is the curvature sum?

The sphere is made of silicon nitride while the ring is made of stainless steel. If the normal applied load is 1,000 N, determine the maximum surface stress, the maximum subsurface stress, the maximum deformation, and the dimension of the contact. That is, determine  $b$ ,  $\mathcal{F}$ ,  $\mathcal{E}$ ,  $t^*$ ,  $D_x$ ,  $D_y$ ,  $\delta_m$ ,  $p_m$ ,  $\tau_0$ ,  $x_0$ , and  $z_0$ .

Also indicate what these values are if the silicon nitride sphere is replaced with a stainless steel sphere. What conclusions can be made about the results? Also compare with Prob. 19.7.1 results.

## 19.8 REFERENCES

- Brewe, D. E., and Hamrock, B. J. (1977): Simplified Solution for Elliptical Contact Deformation Between Two Elastic Solids. *J. Lubr. Technol.*, vol. 99, no. 4, pp. 485-487.
- Hamrock, B. J., and Anderson, W. J. (1973): Analysis of an Arched Outer-Race Ball Bearing Considering Centrifugal Forces. *J. Lubr. Technol.*, vol. 95, no. 3, pp. 265-276.
- Hamrock, B. J., and Brewe, D. E. (1983): Simplified Solution for Stresses and Deformations. *J. Lubr. Technol.*, vol. 105, no. 2, pp. 171-177.
- Hamrock, B. J., and Dowson, D. (1981): *Ball Bearing Lubrication—The Elastohydrodynamics of Elliptical Contacts*. Wiley-Interscience, New York.
- Harris, T. A. (1966): *Rolling Bearing Analysis*. Wiley, New York.
- Hertz, H. (1881): The Contact of Elastic Solids. *J. Reine Angew. Math.*, vol. 92, pp. 156-171.
- Jones, A. B. (1946): *New Departure Engineering Data; Analysis of Stresses and Deflections*. Vols. I and II, General Motors, Inc., Detroit, Michigan.
- Lundberg, G., and Palmgren, A. (1947): Dynamic Capacity of Rolling Bearings. *Acta Polytech., Mech. Eng. Sci.*, vol. 1, no. 3, pp. 6-9.
- Timoshenko, S. P., and Goodier, J. N. (1970): *Theory of Elasticity*, 3d ed. McGraw-Hill, New York.

# CHAPTER 20

## GENERAL SOLUTION FOR STRESSES AND DEFORMATIONS IN DRY CONTACTS

The previous chapter described simple formulas for the maximum surface and subsurface stresses as well as the maximum deformation at the contact center. This chapter defines the stresses and the deformations in a more general manner. As in the previous chapter the contacts are assumed to be dry, or unlubricated.

When two elastic solids like those shown in Fig. 19.1 are brought into contact and subjected to a normal load, the solids deform and the nominal point of contact becomes an elliptical area. Two limiting cases can be identified from this general principle. In the first, a point contact becomes a circle, for example, when the solid surfaces are a sphere on a sphere, a sphere on a plane, or identical cylinders crossed at right angles. In the second limiting case, a nominal line contact becomes a rectangle, for example, when the solid surfaces are a cylinder on a cylinder with parallel axes, a cylinder on a plane, or a cylinder in a groove with parallel axes as in a journal. The stresses, deformations, and contact dimensions are presented here for normal loaded contacts with no tangential loading, not only for the general elliptical contact solution but also for the two limiting situations of circular and rectangular contacts.



In this chapter it is assumed that the linear size of the contact area is small relative to the radii of curvature of the contacting solids. This implies that one body can be replaced by an elastic semi-infinite space. The second assumption imposed in this chapter is that the friction forces arising between touching bodies are neglected.

## 20.1 GENERAL ELASTICITY THEOREMS

The behavior of an isotropic and homogeneous perfectly elastic material is generally defined by equilibrium conditions in which the body forces have been made equal to zero. Imposing these conditions yields the following equations:

$$(1 + \nu)\nabla^2\sigma_x + \frac{\partial^2}{\partial x^2}(\sigma_x + \sigma_y + \sigma_z) = 0 \quad (20.1)$$

$$(1 + \nu)\nabla^2\sigma_y + \frac{\partial^2}{\partial y^2}(\sigma_x + \sigma_y + \sigma_z) = 0 \quad (20.2)$$

$$(1 + \nu)\nabla^2\sigma_z + \frac{\partial^2}{\partial z^2}(\sigma_x + \sigma_y + \sigma_z) = 0 \quad (20.3)$$

$$(1 + \nu)\nabla^2\tau_{xy} + \frac{\partial^2}{\partial x \partial y}(\sigma_x + \sigma_y + \sigma_z) = 0 \quad (20.4)$$

$$(1 + \nu)\nabla^2\tau_{yz} + \frac{\partial^2}{\partial y \partial z}(\sigma_x + \sigma_y + \sigma_z) = 0 \quad (20.5)$$

$$(1 + \nu)\nabla^2\tau_{zx} + \frac{\partial^2}{\partial z \partial x}(\sigma_x + \sigma_y + \sigma_z) = 0 \quad (20.6)$$

where

$$\nabla^2 = \frac{\partial^2}{\partial x^2} + \frac{\partial^2}{\partial y^2} + \frac{\partial^2}{\partial z^2} \quad (20.7)$$

The solution to any elasticity problem must satisfy these conditions and the given boundary equations.

## 20.2 LINE LOAD SOLUTION

Figure 20.1 shows the plane polar coordinates used for a line load  $w'_z$  acting in the  $z$  direction in the  $x = 0$  plane on the boundary surface of an elastic half-space. Also shown in this figure are the Cartesian coordinates. A line load

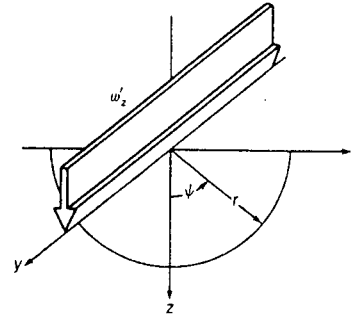


FIGURE 20.1

Plane polar coordinates used for line load  $w'_z$  acting in  $z$  direction in  $x = 0$  plane on boundary surface of elastic half-space. [From Tripp (1985).]

condition is a two-dimensional problem, and the equilibrium conditions for this problem reduce to the following:

$$\frac{\partial\sigma_x}{\partial x} + \frac{\partial\tau_{xz}}{\partial z} = 0 \quad (20.8)$$

$$\frac{\partial\sigma_z}{\partial z} + \frac{\partial\tau_{xz}}{\partial x} = 0 \quad (20.9)$$

$$\left(\frac{\partial^2}{\partial x^2} + \frac{\partial^2}{\partial z^2}\right)(\sigma_x + \sigma_z) = 0 \quad (20.10)$$

Note that Eqs. (20.8) to (20.10) for the two-dimensional problem are much simpler than the three-dimensional equations [(20.1) to (20.6)].

Equations (20.8) to (20.10) may be solved by a "stress function approach," in which  $\phi$ , which is a function of  $x$  and  $z$ , is introduced and expressed in terms of the stresses as

$$\sigma_x = \frac{\partial^2\phi}{\partial z^2} \quad \sigma_z = \frac{\partial^2\phi}{\partial x^2} \quad \tau_{xz} = -\frac{\partial^2\phi}{\partial x \partial z} \quad (20.11)$$

The parameter  $\phi$  is referred to as an Airy stress function. These satisfy Eqs. (20.8) and (20.9) identically, while Eq. (20.10) becomes

$$\frac{\partial^4\phi}{\partial x^4} + 2\frac{\partial^4\phi}{\partial x^2 \partial z^2} + \frac{\partial^4\phi}{\partial z^4} = 0 = \nabla^4\phi \quad (20.12)$$

This is a biharmonic governing equation. To solve a particular problem such as the line load problem, it is necessary to find the appropriate stress function that will satisfy Eq. (20.12) and the appropriate boundary conditions. In many plane problems it is advantageous to express line load in a polar coordinate system as shown in Fig. 20.1 rather than in Cartesian coordinates. Equations (20.8) and

(20.9) become

$$\frac{\partial \sigma_r}{\partial r} + \frac{1}{r} \frac{\partial \tau_{r\psi}}{\partial \psi} + \frac{\sigma_r - \sigma_\psi}{r} = 0 \quad (20.13)$$

$$\frac{1}{r} \frac{\partial \sigma_\psi}{\partial r} + \frac{\partial \tau_{r\psi}}{\partial r} + \frac{2\tau_{r\psi}}{r} = 0 \quad (20.14)$$

The stress function given in Eq. (20.11) can be expressed in polar coordinates as

$$\sigma_r = \frac{1}{r} \frac{\partial \phi}{\partial r} + \frac{1}{r^2} \frac{\partial^2 \phi}{\partial \psi^2} \quad \sigma_\psi = \frac{\partial^2 \phi}{\partial r^2} \quad \tau_{r\psi} = -\frac{\partial}{\partial r} \left( \frac{1}{r} \frac{\partial \phi}{\partial \psi} \right) \quad (20.15)$$

The corresponding biharmonic equation in Eq. (20.12) is expressed in polar coordinates as

$$\left( \frac{\partial^2}{\partial r^2} + \frac{1}{r} \frac{\partial}{\partial r} + \frac{1}{r^2} \frac{\partial^2}{\partial \psi^2} \right) \left( \frac{\partial^2 \phi}{\partial r^2} + \frac{1}{r} \frac{\partial \phi}{\partial r} + \frac{1}{r^2} \frac{\partial^2 \phi}{\partial \psi^2} \right) = 0 \quad (20.16)$$

The line load problem shown in Fig. 20.1 is solved by using the Boussinesq stress function given as

$$\phi_b = -\frac{\omega'_z r \psi}{\pi} \sin \psi \quad (20.17)$$

Substituting Eq. (20.17) into Eq. (20.15) gives

$$\sigma_r = -\frac{2\omega'_z \cos \psi}{\pi r} \quad \sigma_\psi = 0 \quad \tau_{r\psi} = 0 \quad (20.18)$$

This indicates that the stress is radial and directed toward the line where the load is applied. Equations (20.18) are suitable for determining the stress distribution within a semi-infinite solid.

Besides the stresses the surface deformation is also of interest, especially in elastohydrodynamic lubrication studies. It is more convenient to revert to Cartesian coordinates for the deformation considerations. The stress function given in Eq. (20.17) can be expressed in Cartesian coordinates as

$$\phi_b = -\frac{\omega'_z x}{\pi} \tan^{-1} \frac{x}{z} \quad (20.19)$$

The stress field in Cartesian coordinates is

$$\sigma_x = -\frac{2\omega'_z x^2 z}{\pi(x^2 + z^2)^2} \quad (20.20)$$

$$\sigma_z = -\frac{2\omega'_z z^3}{\pi(x^2 + z^2)^2} \quad (20.21)$$

$$\tau_{xz} = \frac{2\omega'_z xz^2}{\pi(x^2 + z^2)^2} \quad (20.22)$$

From Hooke's law the plane strain components in the solids can be expressed as

$$\bar{e}_x = \frac{\partial \delta_x}{\partial x} = \frac{1}{E} [\sigma_x - \nu(\sigma_y + \sigma_z)] \quad (20.23)$$

$$\bar{e}_y = \frac{\partial \delta_y}{\partial y} = 0 = \frac{1}{E} [\sigma_y - \nu(\sigma_z + \sigma_x)] \quad (20.24)$$

$$\bar{e}_z = \frac{\partial \delta_z}{\partial z} = \frac{1}{E} [\sigma_z - \nu(\sigma_x + \sigma_y)] \quad (20.25)$$

$$\bar{e}_{xz} = \frac{\partial \delta_x}{\partial z} + \frac{\partial \delta_z}{\partial x} = \frac{\tau_{xz}}{G_s} = \frac{2(1+\nu)}{E} \tau_{xz} \quad (20.26)$$

where  $G_s$  is the shear modulus of elasticity. From Eq. (20.24), the plane strain condition,

$$\sigma_y = \nu(\sigma_x + \sigma_z) \quad (20.27)$$

Substituting this into Eqs. (20.23) and (20.25) gives

$$\bar{e}_x = \frac{\partial \delta_x}{\partial x} = \frac{1-\nu^2}{E} \sigma_x - \frac{\nu(1+\nu)}{E} \sigma_z \quad (20.28)$$

$$\bar{e}_z = \frac{\partial \delta_z}{\partial z} = \frac{1-\nu^2}{E} \sigma_z - \frac{\nu(1+\nu)}{E} \sigma_x \quad (20.29)$$

Integrating Eqs. (20.28) and (20.29) while making use of Eqs. (20.20) and (20.21) gives

$$\delta_x = -\frac{\omega'_z}{\pi} \left[ \frac{(1-2\nu)(1+\nu)}{E} \tan^{-1} \left( \frac{x}{z} \right) - \frac{(1+\nu)xz}{E(x^2+z^2)} \right] + \bar{A}(z) \quad (20.30)$$

$$\delta_z = -\frac{\omega'_z}{\pi} \left[ \frac{1-\nu^2}{E} \left[ \ln(x^2+z^2) - \frac{z^2}{x^2+z^2} \right] + \frac{\nu(1+\nu)x^2}{E(x^2+z^2)} \right] + \bar{B}(x) \quad (20.31)$$

By symmetry  $-\delta_x(-x) = \delta_x(x)$ . Hence,  $\bar{A}(z) = 0$ .

Equation (20.26) must be used to determine  $\bar{B}(x)$ . That is, substituting Eqs. (20.22), (20.30), and (20.31) into (20.26) gives

$$\frac{\partial \bar{B}(x)}{\partial x} = 0 \quad (20.32)$$

This implies that  $\bar{B}$  is not dependent on the field point  $x$  but does depend on the source point  $\bar{s}$ , in this case chosen at the origin. The value of  $\bar{B}$  is determined by the relative positions of the source and the fixed datum. Therefore, Eqs. (20.30) and (20.31) describe the elastic deformation anywhere in the body due to a line load at the origin. The deformation can be found for any applied surface pressure by an integration method that uses these basic results.

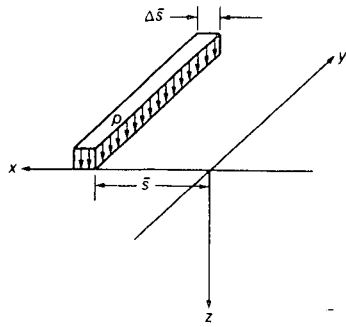


FIGURE 20.2  
Strip of pressure acting as line load.

Only the normal deformation at the surface is usually of interest, but for completeness the general expression is given. From this point on in this text we will only be concerned with normal deformations so that  $\delta = \delta_z$ .

**Sample problem 20.1** Establish what the normal deformation is for a strip of pressure  $p$  and width  $d\bar{s}$  acting on a line on the surface ( $z = 0$ ) at a distance  $\bar{s}$  from the origin ( $x = \bar{s}$ ).

**Solution.** Figure 20.2 shows the strip of pressure that is acting as a line load. In Eq. (20.31) if  $z = 0$ ,  $(x - \bar{s}) \rightarrow x$ , and  $w'_z = p(d\bar{s})$ ,

$$\delta = -\frac{p(d\bar{s})}{\pi} \left\{ \frac{1 - \nu^2}{E} [\ln(x - \bar{s})^2] + \frac{\nu(1 + \nu)}{E} \right\} + \bar{B}$$

When displacements from the distribution of sources are superimposed, they must all be referenced to the *same* datum. Thus, an expression for  $\bar{B}$  is needed inside the integral. The result of integration is  $\bar{C}$ , and it will depend on the choice of the datum.

$$\delta = \frac{-p(d\bar{s})(1 - \nu^2)}{\pi E} \ln(x - \bar{s})^2 + \bar{C}(\bar{s})$$

The displacement due to a variable pressure  $p(\bar{s})$  between  $x = \bar{s}_1$  and  $x = \bar{s}_2$  is found by integrating the preceding equation.

$$\delta = -\frac{1 - \nu^2}{\pi E} \int_{\bar{s}_2}^{\bar{s}_1} \left[ p(\bar{s}) \ln(x - \bar{s})^2 + \bar{C}(\bar{s}) \right] d\bar{s} \quad (20.33)$$

When it is known how the pressure varies, this integral can be evaluated.

In general, one wants to know the displacement of the surface relative to some fixed point beneath the surface, for example, the axis of a cylinder at depth  $R$ . Since the integrand describes only the surface displacements ( $z = 0$ ), it cannot be used to evaluate  $\bar{B}$ . Therefore, the integration will actually involve additional terms in  $z$  that can be obtained from Eq. (20.31). If, on the other hand, the datum can be taken somewhere on the surface itself, it is sufficient to evaluate the integral in Eq. (20.33) and then adjust  $\bar{C}$  by using the integrated results. Thus, the deformation of the surface ( $z = 0$ ) under a uniform pressure  $\bar{p}_c$  extending between

$\bar{s} = -b_2$  and  $\bar{s} = b_2$  is given as

$$\begin{aligned} \delta &= -\frac{(1 - \nu^2)\bar{p}_c}{\pi E} \int_{-b_2}^{b_2} \ln(x - \bar{s})^2 d\bar{s} + \bar{C} \\ &= \frac{(1 - \nu^2)\bar{p}_c}{\pi E} \left[ (x - b_2) \ln(x - b_2)^2 - (x + b_2) \ln(x + b_2)^2 \right] + \bar{D} \quad (20.34) \end{aligned}$$

The preceding equation must be referred to a datum. Setting  $\delta = 0$  at  $x = 0$  and  $z = 0$  while solving for  $\bar{D}$  gives the following:

$$\delta = \frac{2(1 - \nu^2)}{\pi E} \bar{p}_c \left( x \ln \frac{|x - b_2|}{|x + b_2|} - b_2 \ln \frac{|x^2 - b_2^2|}{b_2^2} \right)$$

### 20.3 ELASTIC DEFORMATIONS IN RECTANGULAR CONJUNCTIONS

The general expressions for the deformations in a rectangular conjunction having been developed, these formulas will now be used in elastohydrodynamic lubrication analyses. For two surfaces having the same elasticity but made of different materials coming into contact, Eq. (20.31) gives the elastic deformation at any point  $x$  on the surface ( $z = 0$ ) as

$$\delta = -\frac{2}{\pi E'} \int_{x_{\min}}^{x_{\max}} p \ln(x - x')^2 dx' \quad (20.35)$$

where

$$\frac{1}{E'} = \frac{1}{2} \left( \frac{1 - \nu_a^2}{E_a} + \frac{1 - \nu_b^2}{E_b} \right) \quad (20.36)$$

and  $p$  is pressure that is a function of  $x'$  varying from  $x_{\min}$  to  $x_{\max}$ . Note that since  $\bar{B}$  in Eq. (20.31) depends on the elastic constants, the expression for  $\delta$  in Eq. (20.34) would have an added material-dependent term if the surfaces did not have the same elasticity. Letting

$$\begin{aligned} x &= bX & x' &= bX' & p &= p_H P & \delta &= b^2 \bar{\delta} / R_x \\ \frac{1}{R_x} &= \frac{1}{r_{ax}} + \frac{1}{r_{bx}} & \frac{R_x}{D_x} &= \frac{1}{4} \left( \frac{\pi}{2W'} \right)^{1/2} & W' &= \frac{w'_z}{E'R_x} \quad (20.37) \end{aligned}$$

where  $p_H$  is the maximum Hertzian pressure, causes Eq. (20.35) to become

$$\bar{\delta} = -\frac{1}{2\pi} \left[ \int_{X_{\min}}^{X_{\max}} P \ln(X - X')^2 dX' + \ln \left( R_x^2 \frac{8W'}{\pi} \right) \int_{X_{\min}}^{X_{\max}} P dX' \right] \quad (20.38)$$

But the normal applied load per unit width is just the integration of the pressure from the inlet to the outlet.

$$\therefore w'_z = \int p \, dx$$

This implies that

$$\int P \, dX' = \frac{\pi}{2} \tag{20.39}$$

Substituting Eq. (20.39) into Eq. (20.38) gives

$$\bar{\delta} = -\frac{1}{2\pi} \int_{X_{\min}}^{X_{\text{end}}} P \ln(X - X')^2 \, dX' - \frac{1}{4} \ln\left(R_x^2 \frac{8W'}{\pi}\right) \tag{20.40}$$

Note that the last term on the right side of Eq. (20.40), which is a constant, depends on how  $X$  and  $P$  are made dimensionless. This term represents, in general, 80 to 90 percent of the total deformation. This grouping of the elastic deformation was discovered by Houpert and Hamrock (1986) and proved to be a useful separation in that the remaining pressure-dependent deformation is now of the same order as the film thickness at moderate loads.

Using integration by parts on the integral given in Eq. (20.40), Houpert and Hamrock (1986) found that

$$\bar{\delta} = -\frac{1}{2\pi} |PI|_{X_{\min}}^{X_{\text{end}}} + \frac{1}{2\pi} \int_{X_{\min}}^{X_{\text{end}}} \frac{dP}{dX'} I \, dX' - \frac{1}{4} \ln\left(R_x^2 \frac{8W'}{\pi}\right) \tag{20.41}$$

where

$$I = \int \ln(X - X')^2 \, dX' = -(X - X') [\ln(X - X')^2 - 2] \tag{20.42}$$

Since the pressure is zero at  $X_{\min}$  and  $X_{\text{end}}$ , the first term on the right side of Eq. (20.41) vanishes and

$$\bar{\delta} = -\frac{1}{2\pi} \int_{X_{\min}}^{X_{\text{end}}} \frac{dP}{dX'} (X - X') [\ln(X - X')^2 - 2] \, dX' - \frac{1}{4} \ln\left(R_x^2 \frac{8W'}{\pi}\right) \tag{20.43}$$

The integral in Eq. (20.43) can be calculated analytically by assuming that the pressure is described by a polynomial of second degree in the interval  $[X_{j-1}, X_{j+1}]$ . The details of the calculations are given in Appendix A. The resulting equation from their studies gives the dimensionless deformation  $\bar{\delta}_i$  at node  $i$  as a function of the dimensionless pressure  $P_j$  and the influence coefficients  $D_{ij}$ :

$$\bar{\delta}_i = \sum_{j=1}^N D_{ij} P_j - \frac{1}{4} \ln\left(R_x^2 \frac{8W'}{\pi}\right) \tag{20.44}$$

The results obtained from Houpert and Hamrock (1986) are compared in Table 20.1 with results obtained by Hamrock and Jacobson (1984) as well as by

Okamura (1982), who used simpler approaches than that used by Houpert and Hamrock (1986). Hamrock and Jacobson (1984) assumed the pressure to be constant in the interval  $[X_j - \Delta X/2, X_j + \Delta X/2]$  and used an analytical expression for the integral of  $\ln(X_i - X')$ . Okamura (1982) did not use any analytical solutions and assumed simply that

$$\bar{\delta} = -\frac{\Delta}{2\pi} \sum_{j=1}^N P_j \ln\left(\left|\frac{X_{i+1} + X_i}{2} - X_j\right| \left|\frac{X_{i-1} + X_i}{2} - X_j\right|\right) \tag{20.45}$$

where  $\Delta = X_{i+1} - X_i$ . The three approaches can be compared by assuming a Hertzian pressure. Between  $X = -1$  and  $X = 1$  the film shape while assuming a Hertzian pressure should be flat, leading to  $\Delta H = 0$ , where  $\Delta H$  is defined as

$$\Delta H = \frac{X^2}{2} + \bar{\delta} - \bar{\delta}_m \tag{20.46}$$

and  $\bar{\delta}_m$  is the dimensionless maximum deformation. This can be compared with the value of  $\bar{\delta}_H$  obtained by analytic integration of Eq. (20.40) with a Hertzian pressure distribution.

$$\bar{\delta}_H = -\frac{1}{4} \ln\left(R_x^2 \frac{8W'}{\pi}\right) + \frac{1}{2} \ln(2) + 0.25 \tag{20.47}$$

The largest value  $\Delta H_m/H_m$  of  $\Delta H/H_m$  is found at  $X = -1$  and  $X = 1$  (because of the slope discontinuity) and is shown in Table 20.1 with the corresponding value of  $\bar{\delta}_m/\bar{\delta}_H - 1$ . The film thickness  $H_m$  where  $dP/dX = 0$  has been chosen to be equal to 0.5;  $X_{\min}$  and  $X_{\max}$  define the first and last values of  $X$ ;  $N_{\max}$  is the number of nodes.

Table 20.1 shows that for a given mesh the best accuracy in calculating  $\bar{\delta}$  and  $\Delta H_m$  is obtained by using the Houpert and Hamrock (1986) approach. The value of  $\bar{\delta}_m$  from Hamrock and Jacobson (1984) is in some cases less accurate than that from Okamura (1982) because they did not separate the constant as

TABLE 20.1  
Three ways of calculating elastic deformations

[From Houpert and Hamrock (1986); OK denotes Okamura (1982); HJ denotes Hamrock and Jacobson (1984); HH denotes Houpert and Hamrock (1986).]

$N_{\max}$	$X_{\min}$	$X_{\text{end}}$	$(\bar{\delta}_m/\bar{\delta}_H - 1)$			$\Delta H_m/H_m$		
			OK	HJ	HH	OK	HJ	HH
51	-1.0	1.0	$-1.9 \times 10^{-3}$	$-2.7 \times 10^{-3}$	$8.6 \times 10^{-7}$	$9.4 \times 10^{-3}$	$-5.5 \times 10^{-3}$	$2.7 \times 10^{-3}$
51	-3.6	1.4	$-4.9 \times 10^{-3}$	$-1.1 \times 10^{-2}$	$1.0 \times 10^{-5}$	$3.4 \times 10^{-2}$	$-1.6 \times 10^{-2}$	$8.6 \times 10^{-3}$
151	-1.0	1.0	$-6.3 \times 10^{-4}$	$-5.1 \times 10^{-4}$	$5.1 \times 10^{-8}$	$4.0 \times 10^{-3}$	$-1.4 \times 10^{-3}$	$-6.4 \times 10^{-4}$
151	-3.6	1.4	$-1.6 \times 10^{-3}$	$-2.0 \times 10^{-3}$	$5.4 \times 10^{-7}$	$1.2 \times 10^{-2}$	$-4.4 \times 10^{-3}$	$-2.1 \times 10^{-3}$
301	-1.0	1.0	$-3.1 \times 10^{-4}$	$-1.8 \times 10^{-4}$	$8.1 \times 10^{-9}$	$2.2 \times 10^{-3}$	$-5.6 \times 10^{-4}$	$-2.5 \times 10^{-4}$
301	-3.6	1.4	$-7.8 \times 10^{-4}$	$-7.1 \times 10^{-4}$	$9.0 \times 10^{-8}$	$6.0 \times 10^{-3}$	$-1.8 \times 10^{-3}$	$8.6 \times 10^{-4}$
661	-3.6	1.4	-----	$2.2 \times 10^{-6}$	-----	-----	$-2.6 \times 10^{-4}$	-----
51	-1.0	1.0	-----	-----	$6.5 \times 10^{-7}$	-----	-----	$-2.7 \times 10^{-4}$

<sup>a</sup>Nonuniform.

was done in Eq. (20.40). But  $\bar{\delta}_m$  is not really significant, since any inaccuracy in its calculation can be compensated for by  $H_0$  in the film thickness equation. The important parameter of Table 20.1 is  $\Delta H_m$ , since it is a measure of the flatness of the film. This aspect is extremely important at high loads, where the elastic deformations are two or three orders of magnitude larger than the film thickness.

Also shown in Table 20.1 are the results obtained with a uniform mesh of 661 nodes by Hamrock and Jacobson (1984). Extremely small values of  $\Delta H_m$  were calculated and cannot be reproduced with the new approach because of storage problems with the matrix  $D_{ij}$  and because a large system of equations would have to be solved with such a mesh. By using a nonuniform mesh with a fine grid near  $X = -1$  and  $X = 1$ , similar results were found with a small value of  $N_{\max}$  ( $N_{\max} = 51$ ), as indicated in Table 20.1. The latter case illustrates the power of the approach developed by Houpert and Hamrock (1986).

## 20.4 POINT LOAD SOLUTION

The stress tensor for the problem of a concentrated point load acting along the normal to the undeformed plane surface of an elastic half-space is chosen as the starting point. Because of symmetry the coordinates best suited for these considerations are the cylindrical system  $(r, \theta, z)$  shown in Fig. 20.3.

Consider a point load  $w_z$  acting along the positive  $z$  axis on the boundary surface ( $z = 0$ ) of an elastic half-space defined by  $z > 0$  and having modulus of elasticity  $E$  and Poisson's ratio  $\nu$ . By symmetry, polar angle  $\theta$  does not appear in the stress tensor, and the shear stress components  $\tau_{r\theta}$  and  $\tau_{\theta z}$  vanish. The four remaining stresses can be obtained from Timoshenko and Goodier (1951) as

$$\sigma_r = \frac{w_z}{2\pi} \left\{ (1 - 2\nu) \left[ \frac{1}{r^2} - \frac{z}{r^2(r^2 + z^2)^{1/2}} \right] - \frac{3zr^2}{(r^2 + z^2)^{5/2}} \right\} \quad (20.48)$$

$$\sigma_z = -\frac{3w_z z^3}{2\pi(r^2 + z^2)^{5/2}} \quad (20.49)$$

$$\sigma_\theta = \frac{w_z(1 - 2\nu)}{2\pi} \left[ -\frac{1}{r^2} + \frac{z}{r^2(r^2 + z^2)^{1/2}} + \frac{z}{(r^2 + z^2)^{3/2}} \right] \quad (20.50)$$

$$\tau_{rz} = -\frac{3w_z r z^2}{2\pi(r^2 + z^2)^{5/2}} \quad (20.51)$$

Note that  $(r^2 + z^2)^{1/2}$  is the distance from the point where the load is applied. The stress components given in Eqs. (20.48) to (20.51) satisfy the general requirements of mechanical equilibrium and compatibility. These equations and this physical situation can be likened to the line load solution given in Eqs. (20.20) to (20.22).

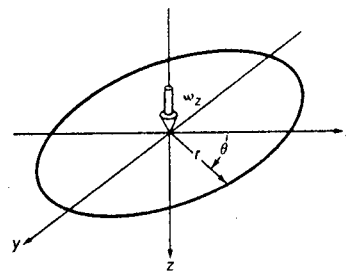


FIGURE 20.3  
Cylindrical polar coordinates used for point load  $w_z$  acting in  $z$  direction at origin on bounding surface of elastic half-space. [From Tripp (1985).]

The deformations in the direction of increasing  $(r, \theta, z)$  compatible with Eqs. (20.48) to (20.51) are

$$\delta_r = \frac{(1 - 2\nu)(1 + \nu)w_z}{2\pi Er} \left[ \frac{z^2}{(r^2 + z^2)^{1/2}} - 1 + \frac{1}{1 - 2\nu} \frac{r^2 z}{(r^2 + z^2)^{3/2}} \right] \quad (20.52)$$

$$\delta_\theta = 0 \quad (20.53)$$

$$\delta_z = \frac{w_z}{2\pi E} \left[ \frac{(1 + \nu)z^2}{(r^2 + z^2)^{3/2}} + \frac{2(1 - \nu^2)}{(r^2 + z^2)^{1/2}} \right] \quad (20.54)$$

From these equations note that  $\delta_r$  and  $\delta_z$  are singular at the origin.

The preceding equations reduce to the following on the surface of the solids, or when  $z = 0$ :

$$\delta_r = -\frac{(1 - 2\nu)(1 + \nu)w_z}{2\pi Er} \quad (20.55)$$

$$\delta_z = \frac{w_z(1 - \nu^2)}{\pi Er} \quad (20.56)$$

Equations (20.48) to (20.56) suggest that for small values of  $r$ , infinite stresses and displacements occur. This is physically impossible, and this purely mathematical condition is avoided by assuming that the point loading is replaced by a hemispherical stress distribution that is equivalent to the load  $w_z$ .

## 20.5 LOADING ON A SEMI-INFINITE BODY

Consider a circular area of radius  $a$  over which a pressure acts. The deformation at point  $M$  outside the circle is shown in Fig. 20.4. From the figure

$$\text{Area of element} = (d\bar{s})(\bar{s}d\psi)$$

$$\text{Load on element} = p\bar{s}d\bar{s}d\psi$$

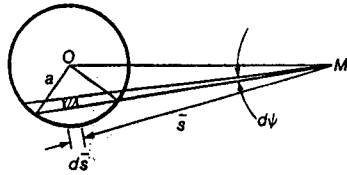


FIGURE 20.4 Deformation outside circular area of radius  $a$  where pressure  $p$  acts. [From Tripp (1985).]

Substituting these into Eq. (20.56) gives

$$\delta_z = p(ds)(d\psi) \frac{1 - \nu^2}{\pi E}$$

Therefore, the total deflection due to all the elements of the loaded area is

$$\delta_z = \frac{1 - \nu^2}{\pi E} \iint p d\bar{s} d\psi \quad (20.57)$$

This equation is valid regardless of the shape of the loaded area.

Figure 20.5 illustrates the situation when  $M$  lies within the loaded area. From the triangle  $Omn$

$$mn = 2a \cos \theta$$

Also from  $OmM$  and from the law of sines, when  $OM = r$

$$\frac{r}{\sin \theta} = \frac{a}{\sin \psi}$$

or

$$\sin \theta = \frac{r}{a} \sin \psi \quad (20.58)$$

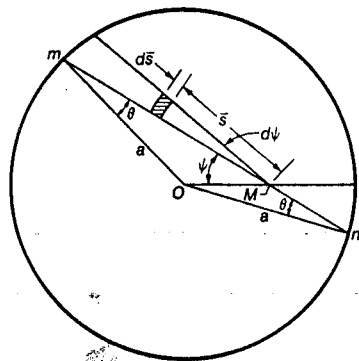


FIGURE 20.5 Deformation inside circular area of radius  $a$  where pressure  $p$  acts. [From Tripp (1985).]

Hence,  $\int d\bar{s}$  over the length  $mn$  is

$$\int_0^{2a \cos \theta} d\bar{s} = 2a \cos \theta$$

Therefore,

$$\iint d\bar{s} d\psi = 2a \int_{-\pi/2}^{\pi/2} \cos \theta d\psi$$

From Eq. (20.58)

$$\cos \theta = (1 - \sin^2 \theta)^{1/2} = \left[ 1 - \left( \frac{r}{a} \right)^2 \sin^2 \psi \right]^{1/2}$$

$$\therefore \iint d\bar{s} d\psi = 2a \int_{-\pi/2}^{\pi/2} \left[ 1 - \left( \frac{r}{a} \right)^2 \sin^2 \psi \right]^{1/2} d\psi$$

Making use of Eq. (20.56) gives

$$\delta_z = \frac{4(1 - \nu^2)}{\pi E} pa \int_0^{\pi/2} \left[ 1 - \left( \frac{r}{a} \right)^2 \sin^2 \psi \right]^{1/2} d\psi \quad (20.59)$$

This integral can be evaluated by using tables of elliptic integrals for any particular value of  $r/a$ .

At the center of the circle when  $r = 0$  ( $OM = 0$ ), the maximum deflection is

$$(\delta_z)_{\max} = \frac{4(1 - \nu^2)}{\pi E} pa \frac{\pi}{2} = \frac{2pa(1 - \nu^2)}{E} \quad (20.60)$$

Note also if  $r = a$ , from Eq. (20.59)

$$(\delta_z)_{r=a} = \frac{4(1 - \nu^2)}{\pi E} pa \int_0^{\pi/2} \cos \psi d\psi = \frac{4(1 - \nu^2)pa}{E\pi} \quad (20.61)$$

$$\therefore (\delta_z)_{r=a} = \frac{2}{\pi} (\delta_z)_{\max} \quad (20.62)$$

Consider the stress at a point on the  $\bar{s}$  axis that is produced by an element ring of pressure on the surface as shown in Fig. 20.6. From Eq. (20.49) the normal stress in the  $\bar{s}$  direction can be expressed as

$$\sigma_z = -\frac{3w_z z^3}{2\pi} (r^2 + \bar{s}^2)^{-5/2} \quad (20.63)$$

Now if  $w_z = 2\pi r p dr$ , this equation becomes, due to the element,

$$\sigma_z = -3pr\bar{s}^3 (r^2 + \bar{s}^2)^{-5/2} dr$$

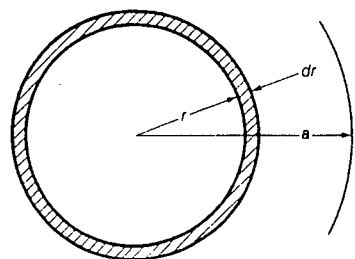


**FIGURE 20.6**  
Ring of pressure on surface of circular area of constant pressure.

The normal stress produced by the entire distributed load is

$$\sigma_z = -3p\bar{s}^3 \int_0^a r(r^2 + \bar{s}^2)^{-5/2} dr = p \left[ 2^3(a^2 + \bar{s}^2)^{-3/2} - 1 \right] \quad (20.64)$$

Note that as  $\bar{s} = 0$ ,  $\sigma_z = -p$ .

The stresses  $\sigma_r$  and  $\sigma_\theta$  at axial points can be calculated while transforming the stress tensor from cylindrical to Cartesian coordinates to give  $\tau_{r\theta} = 0$  and

$$\sigma_r = \sigma_\theta = \frac{p}{2} \left\{ -2(1 + \nu) + \frac{2(1 + \nu)\bar{s}}{(a^2 + \bar{s}^2)^{1/2}} - \left[ \frac{\bar{s}}{(a^2 + \bar{s}^2)^{1/2}} \right]^3 \right\} \quad (20.65)$$

## 20.6 ELASTIC DEFORMATIONS IN ELLIPTICAL CONJUNCTIONS

Figure 20.7 shows a rectangular area of uniform pressure with the appropriate coordinate system. From Eq. (20.56) the elastic deformation at a point  $(x, y)$  of a semi-infinite solid subjected to a pressure  $p$  at the point  $(x_1, y_1)$  can be written as

$$d\delta_z = \frac{2p dx_1 dy_1}{\pi E' r}$$

The elastic deformation at a point  $(x, y)$  due to a uniform pressure over a rectangular area  $2\bar{a} \times 2\bar{b}$  is

$$\delta_z = \frac{2P}{\pi} \int_{-\bar{a}}^{\bar{a}} \int_{-\bar{b}}^{\bar{b}} \frac{dx_1 dy_1}{[(y - y_1)^2 + (x - x_1)^2]^{1/2}} \quad (20.66)$$

where  $P = p/E'$ . Integrating gives

$$\delta_z = \frac{2}{\pi} PD^* \quad (20.67)$$

where

$$\begin{aligned} D^* = & (x + \bar{b}) \ln \frac{(y + \bar{a}) + [(y + \bar{a})^2 + (x + \bar{b})^2]^{1/2}}{(y - \bar{a}) + [(y - \bar{a})^2 + (x + \bar{b})^2]^{1/2}} \\ & + (y + \bar{a}) \ln \frac{(x + \bar{b}) + [(y + \bar{a})^2 + (x + \bar{b})^2]^{1/2}}{(x - \bar{b}) + [(y + \bar{a})^2 + (x - \bar{b})^2]^{1/2}} \\ & + (x - \bar{b}) \ln \frac{(y - \bar{a}) + [(y - \bar{a})^2 + (x - \bar{b})^2]^{1/2}}{(y + \bar{a}) + [(y + \bar{a})^2 + (x - \bar{b})^2]^{1/2}} \\ & + (y - \bar{a}) \ln \frac{(x - \bar{b}) + [(y - \bar{a})^2 + (x - \bar{b})^2]^{1/2}}{(x + \bar{b}) + [(y - \bar{a})^2 + (x + \bar{b})^2]^{1/2}} \end{aligned} \quad (20.68)$$

Hamrock and Dowson (1974) used the preceding equations in their elliptical elasticity analysis as part of their treatment of elastohydrodynamic lubrication. As can be seen from Eq. (20.66), the pressure on each element can be replaced by a constant value; that is, the whole pressure distribution is replaced by blocks of uniform pressure. In this way an analytical expression for integrating the deformation is worked out, and the deformation of every node is expressed as a linear combination of the nodal pressures. In the solution of Ranger et al. (1975), a bilinear interpolating function is used to approximate the practical pressure distribution. Evans and Snidle (1982) employed a different method that was first presented by Biswas and Snidle (1977). For grid elements without singularity they directly adopted Simpson's integration rule, and for those with singularity they used a biquadratic polynomial function to express the pressure distribution approximately. In this way an analytical solution for the integration is developed without directly expressing the deformation as a linear combination of the nodal pressure. Following in these footsteps Hou et al. (1985) employed the biquadratic polynomial function for approaching the pressure distribution on any grid element. An influence coefficient matrix is introduced to reduce the amount of calculating work when repeated calculations of the elastic deformation are needed. However, a shortcoming of their work is that for a  $(2n + 1)(2m + 1)$  finite difference grid, the influence matrix is composed of  $(n \times m)(2n \times 2m \times 9)$  elements, which is not welcomed even with today's powerful computers.

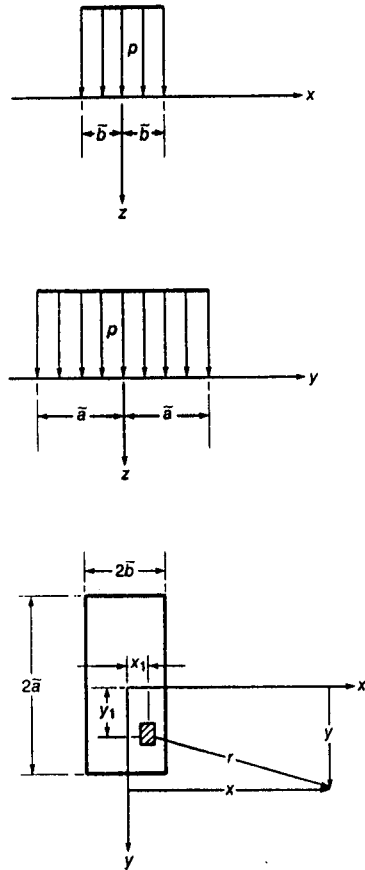


**FIGURE 20.7** Surface deformation of semi-infinite body subjected to uniform pressure over rectangular area. [From Hamrock and Dowson (1981).]

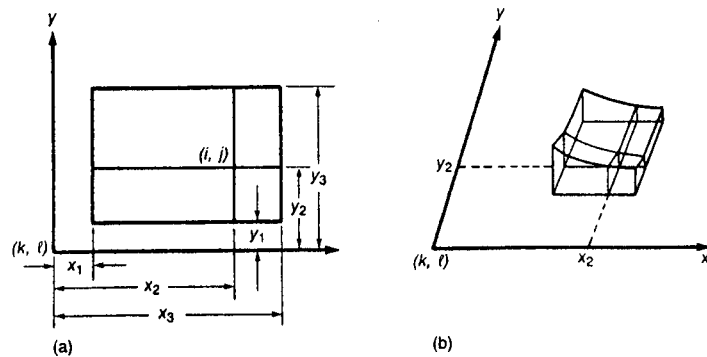


**FIGURE 20.8** Coordinate system for computing element. (a) Rectangular element with nine nodes; (b) representation of pressure distribution for paraboloidal surfaces. [From Jeng and Hamrock (1987).]

Jeng and Hamrock (1987) used a biquadratic polynomial expressed in Lagrange form to approximate the pressure distribution on all grid elements. Figure 20.8 shows the coordinate system for the computing element. Node  $(k, l)$  is the nodal point for the elastic deformation, and node  $(i, j)$  is the central point of the grid element for the pressure distribution. An influence matrix whose coefficient is dependent on the geometric factors and the distance between node  $(k, l)$  and node  $(i, j)$  is introduced only to express the deformation of every node as a linear combination of the nodal pressures. In this way, only  $(2n \times 2m \times 9)$  elements are needed in the influence matrix for a  $(2n + 1)$   $(2m + 1)$  equidistant rectangular grid. The computational time and computer storage size for the influence coefficient matrix are greatly reduced.

### 20.7 CLOSURE

Stresses and deformations in nonconformal conjunctions were presented in a general manner, describing what occurs on as well as within the solids in contact. The conjunctions considered were assumed to be dry, or unlubricated, as in the preceding chapter. The material presented in this chapter is the foundation that will be used extensively in later chapters on elastohydrodynamic lubrication.

A line (two-dimensional) load situation was presented. The general stress equations were solved by a stress function approach that resulted in a biharmonic governing equation. This equation was solved by using the Boussinesq stress function. Thus, not only general expressions for the stresses but also the deformation of the surfaces could be obtained. These general line-contact formulations were then reduced to define the elastic deformation on the surfaces resulting from a rectangular contact area. An important result is that a constant term in the elastic deformation equation accounted for 80 to 90 percent of the total deformation. Isolating this term is thus important in accurately solving for the deformation of solids that have rectangular contact areas. These results will be directly applicable when dealing with elastohydrodynamic lubrication of rectangular conjunctions in Chap. 21.

A point (three-dimensional) load resulted in a stress tensor acting along the normal to the undeformed plane surface of an elastic half-space. The results indicate that for a small radius infinite stresses and displacements occur. This is physically impossible and is avoided by assuming that the point loading is replaced by a hemispherical stress distribution equivalent to the load. This general formulation of the stresses and deformations was then applied to describing the elastic deformation that results in elliptical contacts. The elastic deformation analysis assumed uniform pressure over a small rectangular area. Thus, the pressure could be placed in front of the integral equation, easing the computation considerably. The resulting equation for the elastic deformation was simply expressed as the pressure multiplied by a distance-influencing function. These results will be used when dealing with elastohydrodynamic lubrication of elliptical conjunctions in Chap. 22.



## 20.8 PROBLEMS

20.8.1 Explain the use of the Airy stress function in the analysis of two-dimensional problems in the theory of elasticity, with reference to both Cartesian and polar coordinates.

20.8.2 A semi-infinite uniform plate has a stress system within it defined by the stress function  $\phi = Br^2\theta$ . The boundary of the plate is the line  $\theta = \pm\pi/2$ , and the plate covers the portion of the plane where  $-\pi/2 \leq \theta \leq \pi/2$  and  $r$  is positive. Find the conditions of stress that apply at the boundary and also the stress  $\sigma_x$ ,  $\sigma_y$ , and  $\tau_{xy}$  at any point, in terms of  $\theta$ . Assume that polar and Cartesian coordinates have the same origin and that  $x = r \sin \theta$  and  $y = r \cos \theta$ . A second stress system equal but opposite in sign is now added to the plate, but it is displaced a distance  $a$  from the first. Thus, the second system is represented by the stress function

$$\phi' = B(r')^2\theta'$$

where  $(r', \theta')$  are referred to an origin at the point  $(a, 0)$  in the  $(r, \theta)$  coordinate system.

Show that the superposition of the boundary stresses of the two systems results in a uniform normal stress spread over the length  $r = 0$  to  $r = a$  and in no other stress.

## 20.9 REFERENCES

- Biswas, S., and Snidle, R. W. (1977): Calculation of Surface Deformation in Point Contact EHD. *J. Lubr. Technol.*, vol. 99, no. 3, pp. 313-317.
- Evans, H. P., and Snidle, R. W. (1982): The Elastohydrodynamic Lubrication of Point Contacts at Heavy Loads. *Proc. Roy. Soc. London, Ser. A*, vol. 382, no. 1782, July 8, pp. 183-199.
- Hamrock, B. J., and Dowson, D. (1974): Numerical Evaluation of Surface Deformation of Elastic Solids Subjected to Hertzian Contact Stress. *NASA Tech. Note D-7774*.
- Hamrock, B. J., and Dowson, D. (1981): *Ball Bearing Lubrication—The Elastohydrodynamics of Elliptical Contacts*. Wiley-Interscience, New York.
- Hamrock, B. J., and Jacobson, B. O. (1984): Elastohydrodynamic Lubrication of Line Contacts. *ASLE Trans.*, vol. 27, no. 4, pp. 275-287.
- Hou, K., Zhu, D., and Wen, S. (1985): A New Numerical Technique for Computing Surface Elastic Deformation Caused by a Given Normal Pressure Distribution. *J. Tribol.*, vol. 107, no. 1, pp. 128-131.
- Houpert, L. G., and Hamrock, B. J. (1986): Fast Approach for Calculating Film Thicknesses and Pressures in Elastohydrodynamically Lubricated Contacts at High Loads. *J. Tribol.*, vol. 108, no. 3, pp. 411-420.
- Jeng, Y. R., and Hamrock, B. J. (1987): The Effect of Surface Roughness on Elastohydrodynamically Lubricated Point Contacts. *ASLE Trans.*, vol. 30, no. 4, pp. 531-538.
- Okamura, H. (1982): A Contribution to the Numerical Analysis of Isothermal Elastohydrodynamic Lubrication. *Tribology of Reciprocating Engines*. D. Dowson et al. (eds.). Butterworths, Guilford, England, pp. 313-320.
- Ranger, A. P., Ettles, C. M. M., and Cameron, A. (1975): The Solution of the Point Contact Elastohydrodynamic Problem. *Proc. Roy. Soc. London, Ser. A*, vol. 346, no. 1645, Oct. 19, pp. 227-244.
- Timoshenko, S., and Goodier, J. N. (1951): *Theory of Elasticity*, 2d ed. McGraw-Hill, New York.
- Tripp, J. (1985): Hertzian Contact in Two and Three Dimensions. *NASA Tech. Paper 2473*.

